THE FLOW OF NEMATIC POLYMERS IN AN ECCENTRIC CYLINDER GEOMETRY: THE INFLUENCE OF CLOSURE APPROXIMATIONS

M. Grosso[*], *P. L. Maffettone*[**], *P. Halin, R. Keunings, V. Legat*

CESAME Unité de Mécanique Appliquée,
Université Catholique de Louvain, Avenue G. Lemaitre 4-6, B-1348, Louvain La-Neuve BELGIUM

[**] *Dipartimento di Scienza dei Materiali ed Ingegneria Chimica,*
Politecnico di Torino, Corso Duca degli Abruzzi 24, I-10129, Torino ITALIA

ABSTRACT

The start-up flow of a nematic rodlike polymer in an eccentric cylinder geometry is studied on the basis of the rigid rod model. The simulations neglect the polymer stress contribution in the momentum equation. The nematic configuration is obtained by integrating the diffusion equation for the orientational distribution function with a Galerkin approach. The predictions are compared with results obtained by introducing different closure approximations. Both a quadratic and a Bingham closure are considered. The comparison shows that the approximations have a qualitative impact on the results.

Keywords: Nematic rodlike polymers; Doi model; closure approximations; eccentric cylinders.

[*] Corresponding author. Present address: Dipartimento di Ingegneria Chimica, Università Federico II di Napoli, Piazzale Tecchio 80, I-80125, Napoli, Italia. Email: grosso@hp3.irc.na.cnr.it

INTRODUCTION

Liquid crystalline polymers (LCPs) represent a class of materials that show a peculiar rheology (e. g., [1]). The modeling of LCPs is still an active field of research; an interesting aspect is the characterization of complex flow situations that are commonly encountered in processing. Recently, Feng and Leal [2] have presented an interesting work, in which they address the problem of complex flow simulation in an eccentric cylinder geometry. The liquid crystalline phase is modeled with a simplified constitutive equation derived from the rigid rod model [3] with the introduction of the quadratic closure approximation [4]. No spatial effects are accounted for, and the flow problem is solved by coupling the equation of motion together with the stress equation and the polymer configuration dynamic equations. The adoption of a closure approximation allows the configuration dynamics to be formulated in terms of the second rank order tensor. The results are very intriguing: The scalar order parameter and the director fields show very complex patterns, and the existence of defects is also highlighted. In order to assess the effect of the closure approximation on the results, Feng *et al*. [5] compared, in a subsequent paper, the results obtained with different closures.

In view of these interesting results, we here wish to ascertain the influence of closure approximations following a different approach. We first analyze the same flow problem studied by Leal and coworkers without making use of closure approximations. To keep the numerical burden low, however, we solve the flow problem by neglecting the polymer stress contribution in the momentum equation. The results are then compared with predictions obtained with simplified formulations

without stress coupling. These predictions are used also to compare with Leal and coworkers to evaluate the effect of the stress coupling on the predictions.

THE MODEL

The start up flow of a nematic polymer in an eccentric cylinder is studied. The system geometry is sketched in Figure 1, and is identical to that considered in [2]. The outer cylinder is stationary, and the inner cylinder starts rotating at t=0 with angular velocity ω. For the sake of comparison, the geometrical parameters are those of Feng and Leal (1997): R_1=3, R_2=10, and e=5 (see Fig. 1 for the nomenclature). Thus, the geometry is characterized by two dimensionless parameters: $\mu=(R_2-R_1)/R_1$ = 7/3 and $\varepsilon=e/R_1$=5/3.

The model consists of the equations of motion combined with the constitutive equation for the polymeric phase. The nematic polymer is described by neglecting any spatial interaction. The equations of motion are:

$$\nabla \cdot \mathbf{v} = 0\,, \tag{1}$$

$$\rho \frac{\partial \mathbf{v}}{\partial t} = -\nabla p + \eta_s \nabla^2 \mathbf{v} + \nabla \cdot \tau\,. \tag{2}$$

In Eq. 2, non-linear convective terms are neglected. In Eqs. 1–2, ρ is the density of the fluid, η_s is the solvent viscosity, **v** is the velocity vector, p is the pressure and τ is the polymer stress. A model for the nematic phase must be chosen to compute the stress tensor. We here refer to the rigid rod model that describes the rod–like molecules as rigid Brownian rods with infinite aspect ratio [3]. At a given position in

the space, the dynamics of an ensemble of rigid rods is formulated in terms of a diffusion equation for the rod orientational distribution function $\psi(\mathbf{u}; t)$:

$$\frac{D\psi}{Dt} = \mathcal{D}_r \frac{\partial}{\partial \mathbf{u}} \cdot \left(\frac{\partial}{\partial \mathbf{u}} \psi + \frac{1}{K_B T} \psi \frac{\partial}{\partial \mathbf{u}} V(\mathbf{u}) \right) - \frac{\partial}{\partial \mathbf{u}} \cdot \left[\psi \left(\mathbf{u} \cdot \nabla \mathbf{v} - \mathbf{u}\,\mathbf{u}\mathbf{u} : \nabla \mathbf{v} \right) \right]. \qquad (3)$$

In Eq. 3, the derivative in the LHS is a Lagrangian derivative, $\mathbf{u}$ is the pseudo–versor, $\frac{\partial}{\partial \mathbf{u}}$ is the gradient over the unit sphere, K_B is the Boltzmann constant, T is the absolute temperature, $\nabla \mathbf{v}$ is the velocity gradient, and $\mathcal{D}_r$ is the average rotational diffusivity.

The nematic potential, $V(\mathbf{u})$, is that of Maier–Saupe [6]:

$$V(\mathbf{u}) = -\frac{3}{2} U\, K_B T\, \mathrm{S}{:}\mathbf{u}\mathbf{u}\,. \qquad (4)$$

In Eq. 4, the second rank order tensor is introduced:

$$\mathbf{S} = \int \psi(\mathbf{u})\, \mathbf{u}\mathbf{u}\, d\mathbf{u}\,. \qquad (5)$$

Once the distribution is known, the stress tensor can be calculated as suggested by Doi and Edwards [7]:

$$\boldsymbol{\tau} = 3\nu K_B T \mathbf{S} - 3\nu K_B T U \left(\mathbf{S} \cdot \mathbf{S} - \mathbf{S} : \mathbf{R} \right) + \frac{\nu K_B T}{2\mathcal{D}_r \left(\nu L^3 \right)^2} \nabla \mathbf{v} : \mathbf{R}\,. \qquad (6)$$

In Eq. 6, ν is the number density of the rod–like molecules, L is the rod length, and $\mathbf{R}$ is the fourth rank order tensor given by

$$\mathbf{R} = \int \psi(\mathbf{u})\, \mathbf{u}\mathbf{u}\mathbf{u}\mathbf{u}\, d\mathbf{u}\,. \qquad (7)$$

The diffusion equation (Eq. 3) and Eqs. 1–2 are made dimensionless by considering as characteristic time the reciprocal of the cylinder angular velocity ω^{-1},

and as characteristic length $\Lambda = R_1/3$. The polymer stress, τ, is made dimensionless with the quantity $\nu K_B T$. In this way, three dimensionless groups are obtained:

$$c = \frac{\nu K_B T}{2\eta_S \mathcal{D}_r},$$

$$Pe = \frac{\omega}{6 D_r}, \tag{8}$$

$$Re = \frac{\rho \omega \Lambda^2}{\eta_S}.$$

In Eqs. 8, the parameter c measures the polymer contribution to the total stress [2], Pe is the Peclet number, and Re is the Reynolds number. Finally, in dimensionless form the equations are:

$$\nabla \cdot \mathbf{v} = 0, \tag{9}$$

$$Re \frac{\partial \mathbf{v}}{\partial t} = -\nabla p + \nabla^2 \mathbf{v} + \frac{c}{Pe} \nabla \cdot \boldsymbol{\tau}, \tag{10}$$

$$\frac{D\psi}{Dt} = \frac{1}{6Pe} \frac{\partial}{\partial \mathbf{u}} \cdot \left(\frac{\partial \psi}{\partial \mathbf{u}} + \frac{\psi}{K_B T} \frac{\partial V(\mathbf{u})}{\partial \mathbf{u}} \right) - \frac{\partial}{\partial \mathbf{u}} \cdot \left[\psi \left(\mathbf{u} \cdot \nabla \mathbf{v} - \mathbf{u} \quad \mathbf{u}\mathbf{u} : \nabla \mathbf{v} \right) \right], \tag{11}$$

$$\tau = \mathbf{S} - U\left(\mathbf{S} \cdot \mathbf{S} - \mathbf{S} : \mathbf{R} \right) + \frac{Pe}{\left(\nu L^3 \right)^2} \nabla \mathbf{v} : \mathbf{R}. \tag{12}$$

The predictions can be obtained by integrating the coupled set of Eqs. 9–12. However, for the sake of numerical simplicity, we here solve the problem in a decoupled fashion. In fact, the molecular model (Eq. 11) is solved numerically without resorting to closure approximation, but, the simulations are carried out by considering pure kinematics conditions (*i.e.* the polymer stress is neglected in Eq. 10). This is equivalent to solve the above equations for c=0. Henceforth, we will

refer to the solutions obtained through this procedure as “exact solutions” just to distinguish from solutions obtained with the use of closure approximations.

The influence of closure approximations is analyzed by replacing Eq. 11 with an equation derived with the so-called Prager procedure [8]. In such a way, the evolution equation for the second rank order tensor is obtained as

$$\frac{d\mathbf{S}}{dt} = -6\mathbf{S} + 2\boldsymbol{\delta} + 6U\left(\mathbf{S}\cdot\mathbf{S} - \mathbf{S}:\mathbf{R}\right) + \mathbf{S}\cdot\nabla\mathbf{v} + \nabla\mathbf{v}^T\cdot\mathbf{S} - 2\nabla\mathbf{v}:\mathbf{R}\,. \tag{13}$$

In Eq. 13, δ represents the second rank unit tensor. In order to “close” Eq. 13, a closure approximation, $\mathbf{R} = \boldsymbol{f}(\mathbf{S})$, is needed. We here use two different closures: the quadratic closure [4], and a Bingham closure ([9–10]). The predictions obtained with closure approximations can give two pieces of information. On one hand, one can compare the results with those obtained with the exact *model* (Eq. 11) to evaluate the impact of the closure approximations when the flow field is prescribed. On the other hand, it is possible to estimate the effect of the c−parameter by comparison with the previous works of Leal and coworkers, who solved the coupled problem with the same types of closure; and, therefore, the importance of the coupling can somehow be evaluated.

The quadratic closure reads:

$$\mathbf{R} = \mathbf{SS}\,. \tag{14}$$

The Bingham closure here adopted has been recently presented in [10], and can be compactly written as:

$$
\begin{aligned}
&\mathrm{R} = \beta_1 \overline{\delta\delta} + \beta_2 \overline{\delta \mathrm{S}} + \beta_3 \overline{\mathrm{SS}} + \beta_4 \overline{\delta \mathrm{S} \cdot \mathrm{S}} + \beta_5 \overline{\mathrm{SS} \cdot \mathrm{S}} + \beta_6 \overline{\mathrm{S} \cdot \mathrm{SS} \cdot \mathrm{S}}, \\
&\beta_1 = \frac{1}{140}\left[7\beta_4 (4I_3 - 3) - \beta_5 (3 + 12I_2 + 56I_3) - 6\left(2 + \beta_6 (1 - I_2 + 8I_3)\right)\right], \\
&\beta_2 = \frac{1}{14}\left[12 + 7\beta_4 + 3\beta_5 (1 + 4I_2) + \beta_6 (6 - 6I_2 - 8I_3)\right], \\
&\beta_3 = \frac{1}{4}\left[-7\beta_4 - 7\beta_5 + 2\beta_6 (4I_2 - 3)\right], \\
&\beta_4 = k_1 + p_1 I_3 + p_2 I_2 + p_3 I_3^{\,2}, \\
&\beta_5 = p_4 + p_5 I_3 + p_6 I_2 + p_7 I_3^{\,2}, \\
&\beta_6 = p_8 + p_9 I_3 + p_{10} I_2 + k_2 I_3^{\,2}.
\end{aligned}
\tag{15}
$$

In the above equations, the overbar implies the tensor symmetrization, and I_2 and I_3 represent the second and the third invariant of tensor **S**:

$$
\begin{aligned}
I_2 &= \frac{1}{2}(1 - \mathbf{S} : \mathbf{S}) \\
I_3 &= Det(\mathbf{S})
\end{aligned}
\tag{16}
$$

The numerical values of the parameters are reported in Table 1.

THE NUMERICAL TECHNIQUES

Equations 9–10 are integrated by adopting a Lagrangian streamline integration. The numerical algorithm is a particular case of the Lagrangian Particle Method (LPM), which combines in a decoupled fashion the solution of the conservation laws with a Lagrangian computation of the polymer configuration (Eqs. 11–12) for a discrete number of particles. In the case at hand the contribution of the polymer stress to the total stress is neglected (i.e. $c = 0$), so that the integration of Equations 9–10 is performed independently of the polymer configuration integration. The latter integration is performed once the flow field has been calculated. Details on LPM may be found elsewhere [11].

The integration of the diffusion equation (Eq. 11) is performed through a Galërkin scheme: The distribution function is expanded as a spherical harmonics series ([12−13])

$$\psi(\mathbf{u},t)=\sum_{\substack{l=0\\ l\,even}}^{\infty}\sum_{m=-l}^{m=l} b_{\mathrm{l,m}}(t)\mathrm{Y}_l^m(\vartheta,\phi)\,, \tag{17}$$

where the b_{lm} coefficients are complex functions of time. The expansion is truncated at some level n and, by exploiting the orthogonality properties of the spherical harmonics, one ends up with a set of ordinary differential equations in terms of the b_{lm} coefficients. In fact, for the parameter values investigated here, numerical convergence has been obtained by truncating the expansion at n=12.

RESULTS AND DISCUSSIONS

The solutions are described by reporting two descriptors of the system: the scalar order parameter and the director angle. There is no rigorous definition of these physical quantities in flow conditions. However, following Larson [14], we consider the scalar order parameter as:

$$S = \sqrt{\frac{3}{2}\mathbf{S}:\mathbf{S}-\frac{1}{2}}\,. \tag{18}$$

The director is defined as the orientation of the eigenvector of **S** corresponding to its largest eigenvalue. As a general result, all our simulations show that the asymptotic solutions do not change as the initial state for the distribution function is varied. The asymptotic state is always characterized by the director lying in the flow plane. As a

consequence, only one angle is needed to describe the director orientation of the regime solutions. This angle is measured with respect to the x−axis.

The parameter to be fixed for the simulations are U, Re, and Pe. Two Peclet numbers are investigated: Pe=10 and Pe=20. The Reynolds number is always 5.55×10^{-5}Pe. The U−value is chosen so to have the same equilibrium condition of Feng and Leal [2], that is a scalar order parameter, S_{eq}, equal to 0.683. For this value of the equilibrium scalar order parameter, only the prolate nematic is stable at rest. The corresponding U−value is 5.392. For future reference, the U−value corresponding to S_{eq}=0.683 for the quadratic closure is U=4, whereas it coincides with that of the exact model for the Bingham closure.

In the following, the director field and the scalar order parameter field, as predicted by Eq. 11 and with closure models, are presented. Only asymptotic solutions are illustrated. The director field is drawn by plotting, as done by Feng and Leal, ellipses that represent the projection of the second rank order tensor onto the flow plane. The largest axis gives the director orientation. The lengths of the axes are proportional to the corresponding **S**−eigenvalues in the xy−plane.

Results without closure approximations

In this section we report the solutions obtained by integrating Eq. 11, that is, without resorting to closure approximations. Figure 2 illustrates the director field for Pe=10. Since the asymptotic solution is periodic in the recirculation zone, the graph is just a snapshot taken during the asymptotic oscillation. The solid line encircles the subdomain in which the periodic oscillation occurs. In this region, the system shows

a wagging–like solution, *i.e.,* the director oscillates between two limiting angles. The director field is here rather complex, but no evidence of defect–like situations are envisaged. Close to the inner cylinder the director is aligned along the streamline directions. Something similar to a defect –1/2 is found on the external cylinder (coordinate), where the director field shows a discontinuity.

Figure 3 shows the scalar order parameter field for the same parameter values of Fig. 2. Several minima and maxima are found. In the recirculation zone, as typical of the wagging regime, the scalar order parameter reaches very low values during the oscillation. Close to the inner cylinder the scalar order parameter shows wide spatial variations. A relative minimum is detected below the inner cylinder on the left, and a relative maximum is present on top of the inner cylinder on the left again. The situation is even more complex on the boundary between the recirculation zone and the region close to the inner cylinder. Two stationary relative minima are found: one in the position $(x, y) \approx (-3,-7)$, the other at $(x, y) \approx (1.2,1.4)$. In the recirculation zone away from the wagging region, the scalar order parameter experiences again wide variations: it is higher in the bulk of the recirculation zone, and lower in the region close to the outer cylinder.

Figures 4–5 report the director field and the scalar order parameter field for Pe = 20, respectively. No significant differences with respect to the lower value of Peclet are found except in the recirculation zone where a stable stationary solution is found. Actually, the asymptotic solution is stationary everywhere. This is coherent with the behavior typical of simple shearing flow where periodic solutions give the

way to stationary solutions as the Peclet number increases [14]. Also in this case, the scalar order parameter is low in the recirculation zone, reaching a minimum of 0.20.

Results with closure approximations

We first present the predictions of both quadratic and Bingham closure approximations for Pe=20 so that a direct comparison with the data of Feng and Leal can be addressed.

Figures 6–7 report the director field and the scalar order parameter field for the quadratic closure. The results are qualitatively and quantitatively close to the results by Feng and Leal (see their Fig. 4d in [2]). The solution is stationary. The director is aligned with the circular streamlines close to the inner cylinder. In the recirculation zone, a defect of strength +1/2 is found as in the work of Feng and Leal. In correspondence of the defect, the scalar order parameter reaches a minimum (S_{min}=0.218), which is very close to the value reported in [2] (S=0.248). The scalar order parameter field is much simpler than that predicted without closure approximations; moreover, the scalar order parameter is clearly overestimated. All these results imply that the stress coupling, at least at the level used by Feng and Leal, does not significantly affect the predictions. On the other hand, the comparison with the results obtained without the closure approximation shows that many qualitative aspects are missed with the quadratic closure. This is obviously not unexpected, as it is well known that this closure gives very poor results also in simple flows.

Figures 8–9 are obtained with the Bingham closure approximation (Eq. 15). The asymptotic solution shows a periodic region in the recirculation zone, thus the plots report only an instantaneous snapshot of the periodic solution. The oscillation in the recirculation zone is complex. Two zones one of the tumbling type, *i. e.*, in a fixed spatial position the director rotates indefinitely in time, and another of the wagging type are encountered. In the figure, the tumbling and the wagging domains are encircled with a solid line. The scalar order parameter field shows some structure. Two maxima and two minima are found close to the inner cylinder. A wide region where the scalar order parameter is rather uniform separates the two tumbling domains. A qualitative agreement with the exact solution (Fig. 4–5) is found in some regions of the flow field. For example, close to the inner cylinder, the closure model is able to correctly reproduce the presence of minima and maxima. In addition, as in Fig. 6, in the recirculation zone, the scalar order parameter S is high in the bulk, and low in the region close to the outer cylinder. On the other hand, the periodic domain found with the Bingham closure is absent in the exact solution.

Since at Pe=10 the Bingham closure predictions do not differ qualitatively from those just shown, no plots of the director and the scalar order parameter field for the closure approximations are reported. Again, two periodic domains of the tumbling type are found. If one compares this situation with the exact solution for Pe=10, it turns out that the agreement is much better. This confirms that the Bingham closures behaves satisfactorily in slow flows ([9–10]).

Local comparison

A quantitative comparison between the constitutive equations can be performed by investigating the dynamics evolution in different points of the flow field. Here, three different positions are monitored: point A close to the inner cylinder ((x,y) = (–2.5,2.5)); point B in the recirculation zone ((x,y)=(2.5, 0)), and point C close to the outer cylinder ((x,y) = (0, –7.5)).

Figures 10–12 report the evolution of the scalar order parameter S and the director angle α at points A, B, and C, respectively, for Pe=10. The exact solution is plotted with solid lines, and the Bingham closure is plotted with dotted lines. The initial condition is always the isotropic condition. For the exact solution this corresponds to

$$\psi(\mathbf{u},0)=\frac{1}{4\pi}, \tag{19}$$

whereas for the simplified formulation it reads:

$$\mathbf{S}(0)=\begin{bmatrix} 1/3 & 0 & 0 \\ 0 & 1/3 & 0 \\ 0 & 0 & 1/3 \end{bmatrix}. \tag{20}$$

The evolution at point A is reported in Figure 10. The asymptotic solution is stationary both for the exact model and the Bingham approximation. The steady state scalar order parameters are very close, whereas a slight discrepancy is found for the director orientation. It is apparent that at this position the exact solution and the Bingham closure are in good agreement

In Figure 11, the evolution for *S* and α are plotted at point B. The exact model predicts a wagging–like solution. The director angle oscillates between two limiting values, and the scalar order parameter oscillates between 0.25 and 0.59. The

Bingham closure gives here a very different picture as it predicts a tumbling–like solution with the scalar order parameter oscillating between the values of 0.52 and 0.865.

Figure 12 shows the evolution of S and α at point C. Both models predict a stationary solution. However, from a quantitative point of view, the Bingham closure predicts a much larger scalar order parameter (0.81 vs. 0.61). A better agreement is found for the director angle.

For Pe= 20, the situation at A and C is very similar to those just illustrated, and thus no plot is presented. Figure 13 shows the situation at point B. The exact solution predicts a stable stationary solution, which is eventually reached after a long transient. On the contrary, the Bingham closure predicts a tumbling regime. This discrepancy is due to the intrinsic nature of this closure approximation that overestimates the range of existence of the periodic regime for U>5 (see [10]).

DISCUSSION

As a general result, it is apparent that the closure approximations investigated here do not describe satisfactorily the dynamics of the exact solution. The Bingham closure performs adequately at low Peclet values as already noted for simple flows [10]. Unfortunately, as the flow field becomes stronger, the quality of the predictions degrades. An explanation of this degradation can be related to the orthotropic nature of the closure [15]. Since the fourth rank order tensor takes all its directional information from the second rank order tensor, it possesses strong symmetry properties, that is, all the off–diagonal components of the fourth rank order tensor

must be zero when written in the eigenspace of second rank order tensor. A possible measure of *orthotropicity* of the exact fourth rank order tensor was suggested in [13]. We slightly modify the proposed norm by normalizing it with the scalar order parameter:

$$norm = \frac{\sqrt{R_{1112}^2 + R_{1222}^2 + R_{1113}^2 + R_{1333}^2 + R_{1233}^2 + R_{1223}^2 + R_{1123}^2 + R_{2223}^2 + R_{2333}^2}}{S}. \quad (21)$$

In Eq. 21, the fourth order tensor is written in the eigenspace of **S**. This norm can be used only with an anisotropic state, and is zero when the orthotropic assumption holds true. Figure 14 reports the value of this norm in the flow field for Pe=20. It is apparent that the orthotropic assumption does not hold true. However, it is worth noting that the Bingham closure gives the best results in the regions where this norm is smaller, *i.e.* in the bulk of the recirculation zone and above on the left of the inner cylinder. Of course, as the Peclet number decreases, the norm of Eq. 20 decreases as well, thus confirming the better agreement found in this work for Pe=10.

It should be mentioned that our simulations have shown that no stable solution is encountered with the director oriented orthogonally to the flow plane (*log–rolling regime*, [12]) in contrast with the results obtained by Feng and Leal [2]. This discrepancy could, of course, be due to the absence of coupling polymer stress coupling in our work. However, the presence of log–rolling solutions in Feng and Leal may also be caused by the constrained symmetries adopted by them. In fact, in their work, the out–of–flow–plane components of the second moment tensor are imposed to be always nil. This means that the director can be oriented only within the flow plane or in the direction orthogonal to it. On the other hand, in the present

work, the model is three–dimensional, *i. e.*, the distribution function and also the second rank order tensor are not restricted by any constraint. Therefore, the director is free to evolve in a 3d space, and it can easily leave the log–rolling orientation. Instead, in the formulation of Feng and Leal, the director can leave the orientation orthogonal to the flow plane only if the configuration passes through a nematic–oblate state (or even isotropic), and, since this route is energetically expensive, the stability of log-rolling solutions is thus enforced with respect to our formulation.

CONCLUSIONS

In the present work, the problem of a complex flow simulation of nematic polymers, described with the rigid –rod model, has been addressed. The main objective of this work was to ascertain whether simplified constitutive equations based on closure approximations are adequate. Two closure approximations have been considered: the quadratic and the Bingham closure. The comparison is made by considering the flow between rotating eccentric cylinders. The flow problem is solved by neglecting the polymer contribution to the stress. Within this assumption, it turns out that the closure approximations cannot be used at large Peclet numbers. The Bingham closure behaves satisfactorily only at low Pe.

The influence of the polymer stress coupling has been qualitatively evaluated by comparing the results obtained with the quadratic closure with those presented by Feng and Leal [2] in the very same situation but with a moderate stress coupling. It

appears that no significant difference was present, thus suggesting that, at least at moderate c–values the impact of the coupling is negligible.

Acknowledgments

The work of M.Grosso has been supported by the ARC 97/02–210 project, Communautè Française de Belgique.

REFERENCES

[1] Burghardt, W. R., "Molecular orientation and rheology in sheared lyotropic liquid crystalline polymers", *Macromol. Chem. Phys.*, 199, 471–488, 1998.

[2] Feng J., Leal L. G., "Simulating complex flows of liquid–crystalline polymers using the Doi theory", *J. Rheol.*, 41, 1317–1335, 1997.

[3] Doi M., "Molecular Dynamics and Rheological Properties of Concentrated Solutions of Rodlike Polymers in Isotropic and Liquid Crystalline Phases", *J. Polym. Sci. Polym. Phys.*, 19, 229–243, 1981.

[4] Hinch E.J. and Leal L.G. J., "Constitutive Equation in Suspension Mechanics. Part 1. General Formulation", *J. Fluid Mech.*, 71, 481–495, 1975.

[5] Feng J., Chaubal C. V., Leal L. G., "Closure approximations for the Doi theory: Which to use in simulating complex flows of liquid–crystalline polymers?", *J. Rheol.*, 42, 1095–1119, 1998.

[6] Maier W. and A. Saupe, “Eine einfache molekular–statistische Theorie der nematischen kristallinflüssigen Phase Teil I”, *Z. Naturforsch. A*, 14**A**, 882–889, 1959.

[7] Doi M., and S.F. Edwards, *The Theory of Polymer Dynamics*, Clarendon Press, Oxford, 1986.

[8] Prager S., “Stress–strain relations in a suspension of dumbbells”, *Trans. Soc. Rheol.*, 1, 53–62, 1957.

[9] Chaubal C. V., and L. G. Leal, “A closure approximation for liquid crystalline polymer models based on parametric density estimation”, *J. Rheol.*, 42, 177–201, 1998.

[10] Grosso M., P. L. Maffettone, F. Dupret, “A closure approximation for nematic liquid crystals based on the canonical distribution subspace theory”, in the press, *Rheol. Acta*, 2000.

[11] Halin P., Lielens G., Keunings R., Legat V., “The Lagrangian particle method for macroscopic and micro-macro viscoelastic flow computations”, *J. Non-Newtonian Fluid Mech.,* 79, 387–403, 1998

[12] Larson R. G. and H. C. Öttinger, “The Effect of Molecular Elasticity on Out–of–Plane Orientations in Shearing Flows of Liquid Crystalline Polymers”, *Macromolecules*, 24, 6270–6282, 1991

[13] Faraoni V., M. Grosso, S. Crescitelli, P. L. Maffettone, “The rigid rod model for nematic polymers: An analysis of the shear flow problem”, *J. Rheol.*, 43, 829–843, 1999.

[14] Larson R.G., “Arrested Tumbling in Shearing Flows of Liquid Crystal Polymers”, *Macromolecules*, 23, 3983–3992, 1990.

[15] Cintra Jr. J. S., Tucker III C. L., “Orthotropic closure approximations for flow induced fiber orientations"” *J. Rheol.* 39, 73–103, 1995.

FIGURE CAPTIONS

Fig. 1 – The eccentric cylinder geometry. Relevant geometrical and kinematic parameters are illustrated.

Fig. 2 – A snapshot of the director field during the oscillating regime for Pe=10 as predicted with the exact solution. The ellipses represent the projection onto the flow plane of the second rank order tensor. The wagging region is encircled.

Fig. 3 – A snapshot of the scalar order parameter field during the oscillating regime for Pe=10 as predicted with the exact solution.

Fig. 4 – The director field at the steady state for Pe=20 as predicted with the exact solution.

Fig. 5 – The scalar order parameter field at the steady state for Pe=20 as predicted with the exact solution.

Fig. 6 – The director field at the steady state for Pe=20 as predicted with the quadratic closure approximation.

Fig. 7 – The scalar order parameter field at the steady state for Pe=20 as predicted with the quadratic closure approximation.

Fig. 8 – A snapshot of the director field during the oscillating regime for Pe=20 as predicted with the Bingham closure approximation. The tumbling region is encircled.

Fig. 9 – A snapshot of the scalar order parameter field during the oscillating regime for Pe=20 as predicted with the Bingham closure approximation.

Fig. 10 – The evolution of the scalar order parameter and the director orientation for Pe=10 at point A (see text). The solid lines represent the exact solutions; the dashed lines represent the predictions of the Bingham closure model.

Fig. 11 – The evolution of the scalar order parameter and the director orientation for Pe=10 at point B (see text). The solid lines represent the exact solutions; the dashed lines represent the predictions of the Bingham closure model.

Fig. 12 – The evolution of the scalar order parameter and the director orientation for Pe=10 at point C (see text). The solid lines represent the exact solutions; the dashed lines represent the predictions of the Bingham closure model.

Fig. 13 – The evolution of the scalar order parameter and the director orientation for Pe=20 at point B (see text). The solid lines represent the exact solutions; the dashed lines represent the predictions of the Bingham closure model.

Fig. 14 – The field of the norm of Eq. 21 for Pe=20.

TABLE 1

p_1	p_2	p_3	p_4	p_5	p_6
–9.6746	–53.486	14.4619	–2.2786	–9.0389	108.098
p_7	p_8	p_9	p_{10}	k_1	k_2
10.6180	–1.3120	14.1101	–68.022	4.5906	*–12.3304*

Figure 1
Grosso et al.

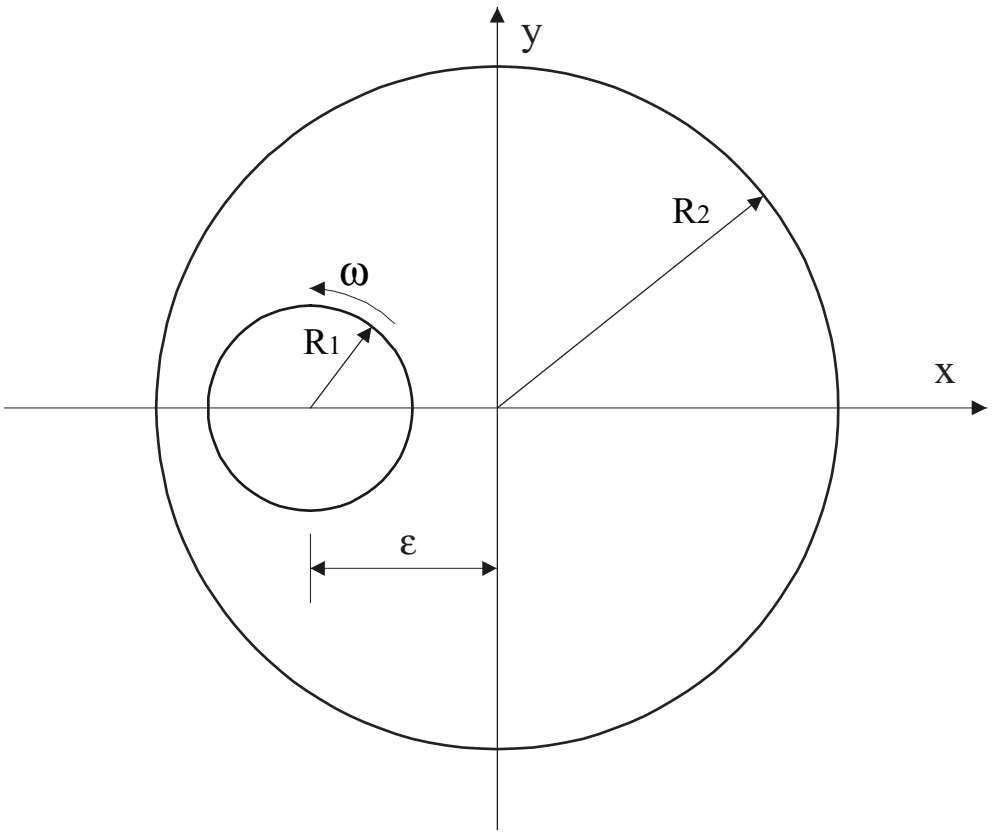

Figure 2
Grosso et al.

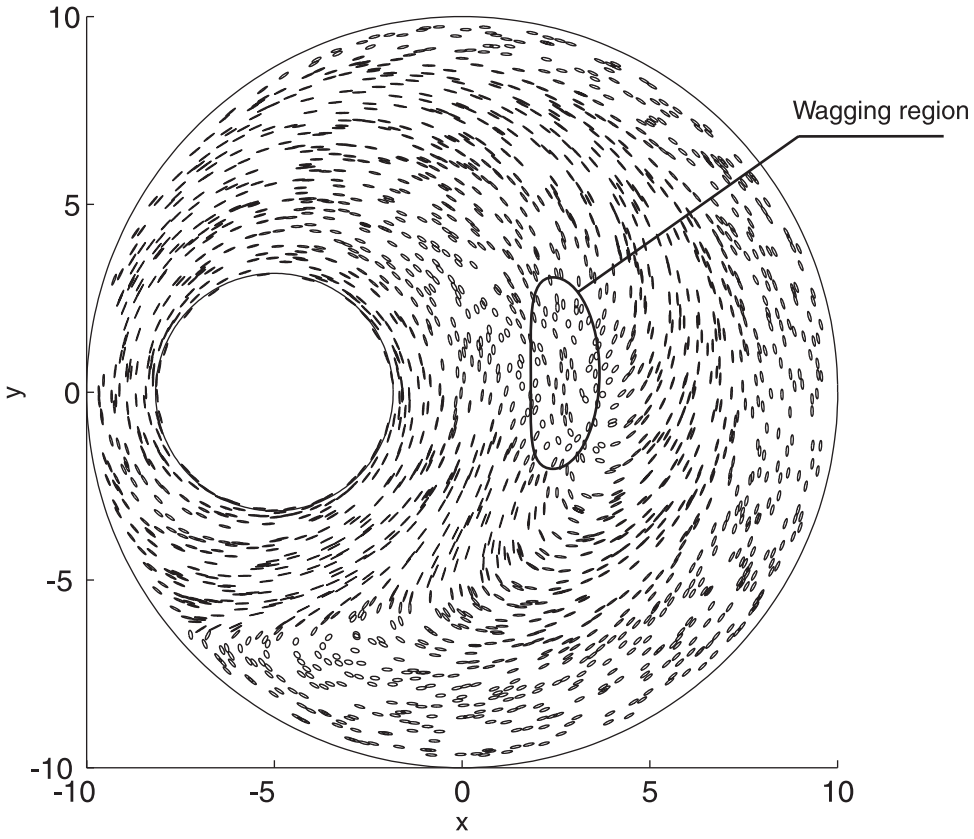

Figure 3
Grosso et al.

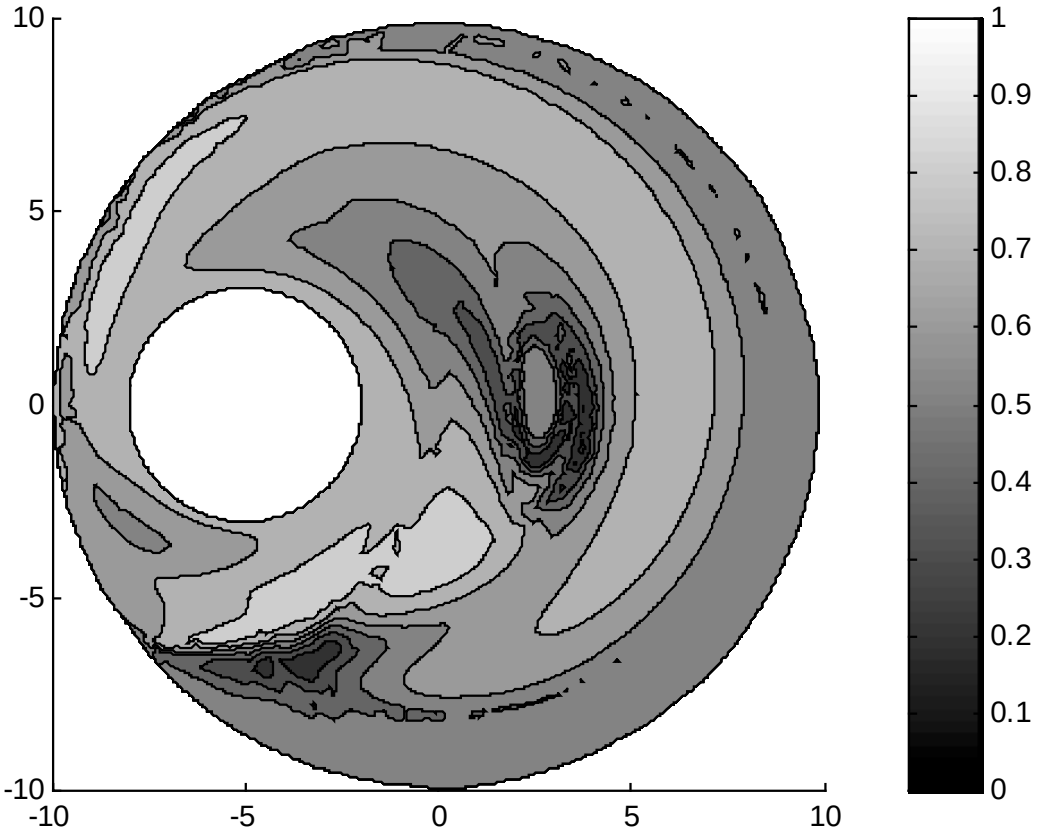

Figure 4
Grosso et al.

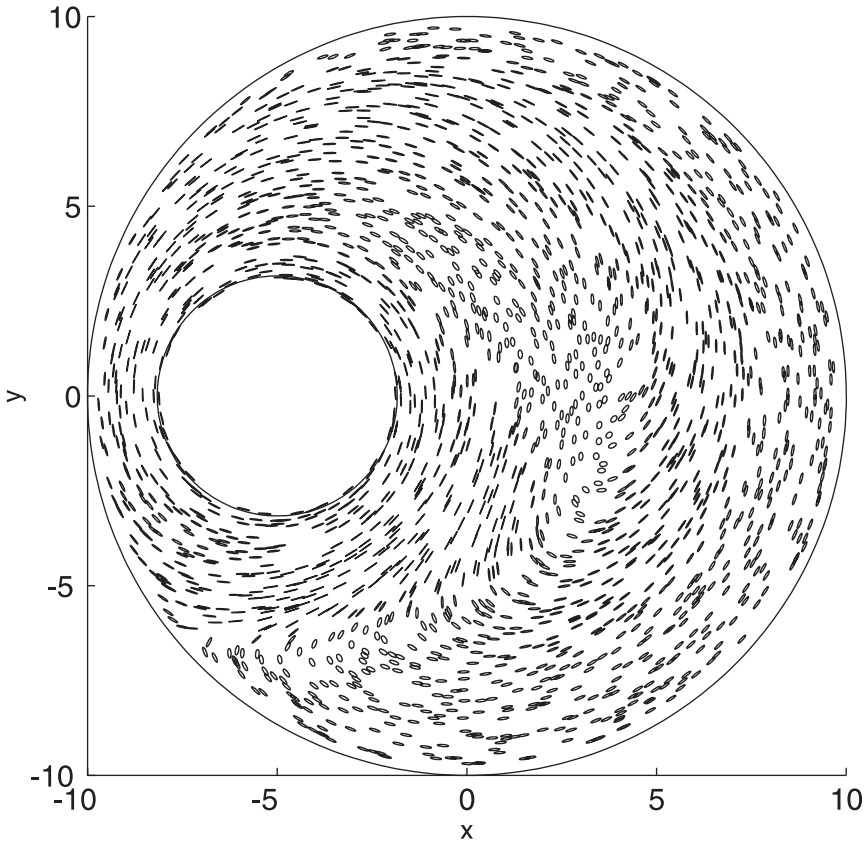

Figure 5
Grosso et al.

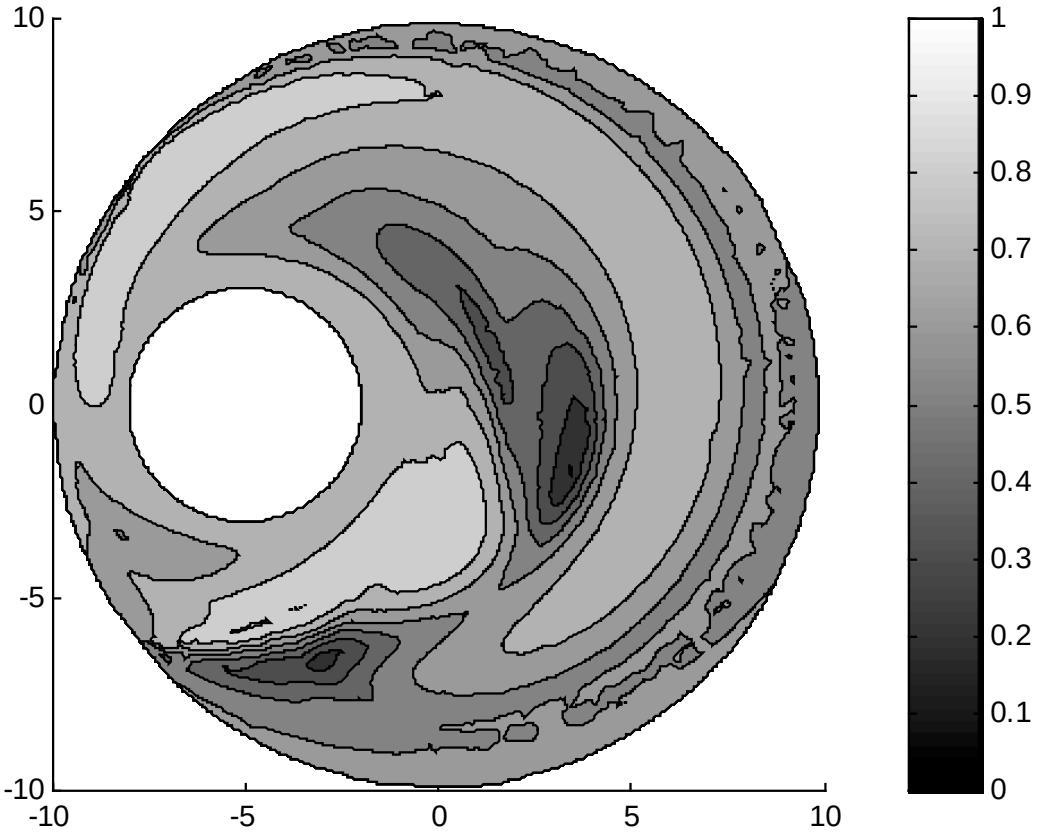

Figure 6
Grosso et al.

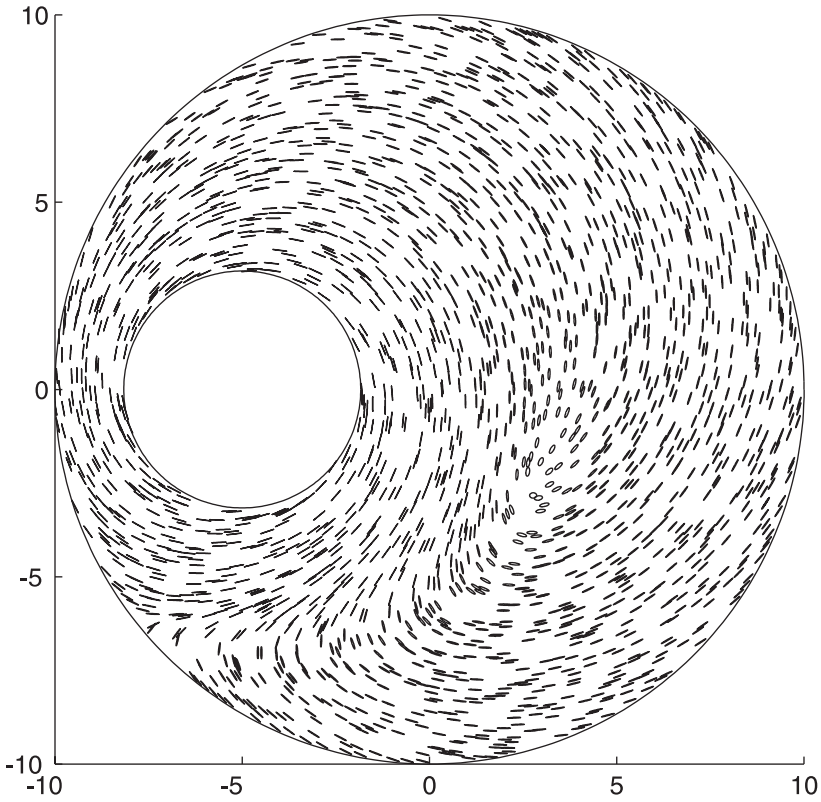

Figure 7
Grosso et al.

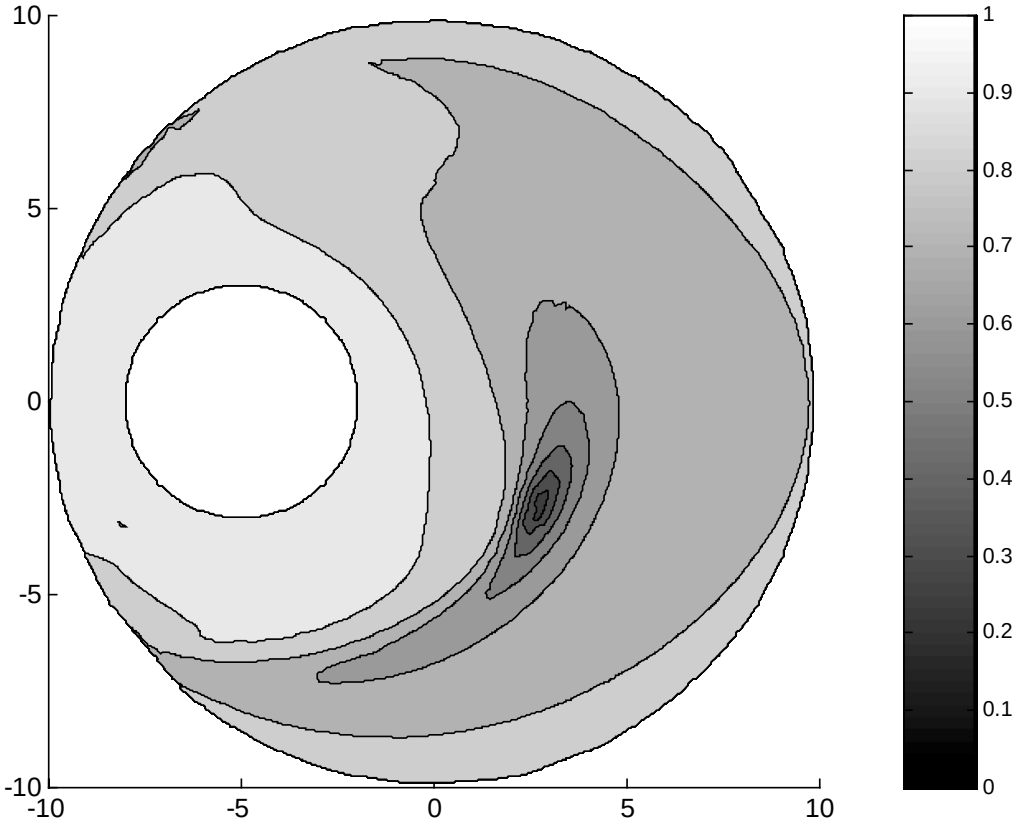

Figure 8
Grosso et al.

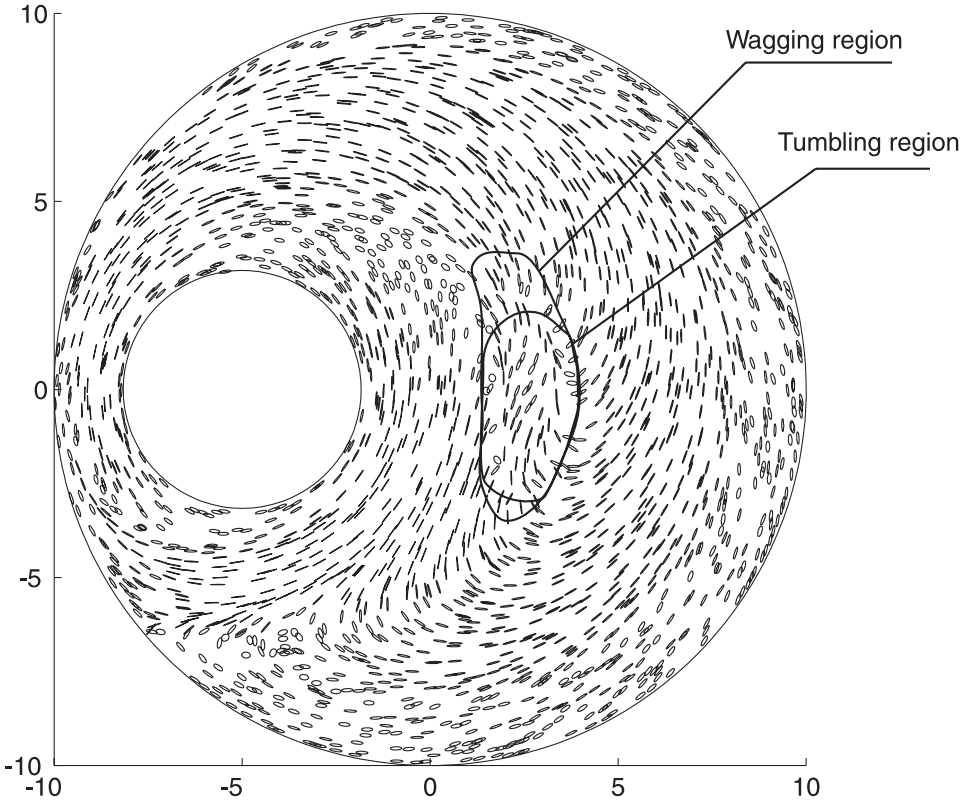

Figure 9
Grosso et al.

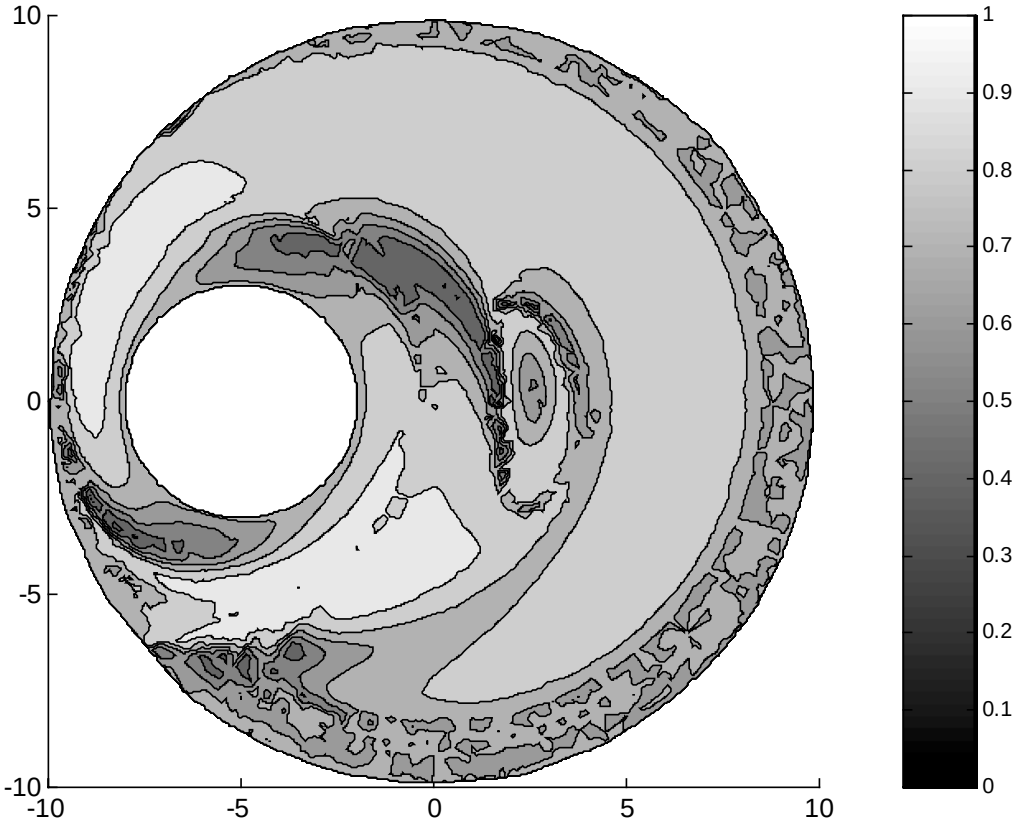

Figure 10
Grosso et al.

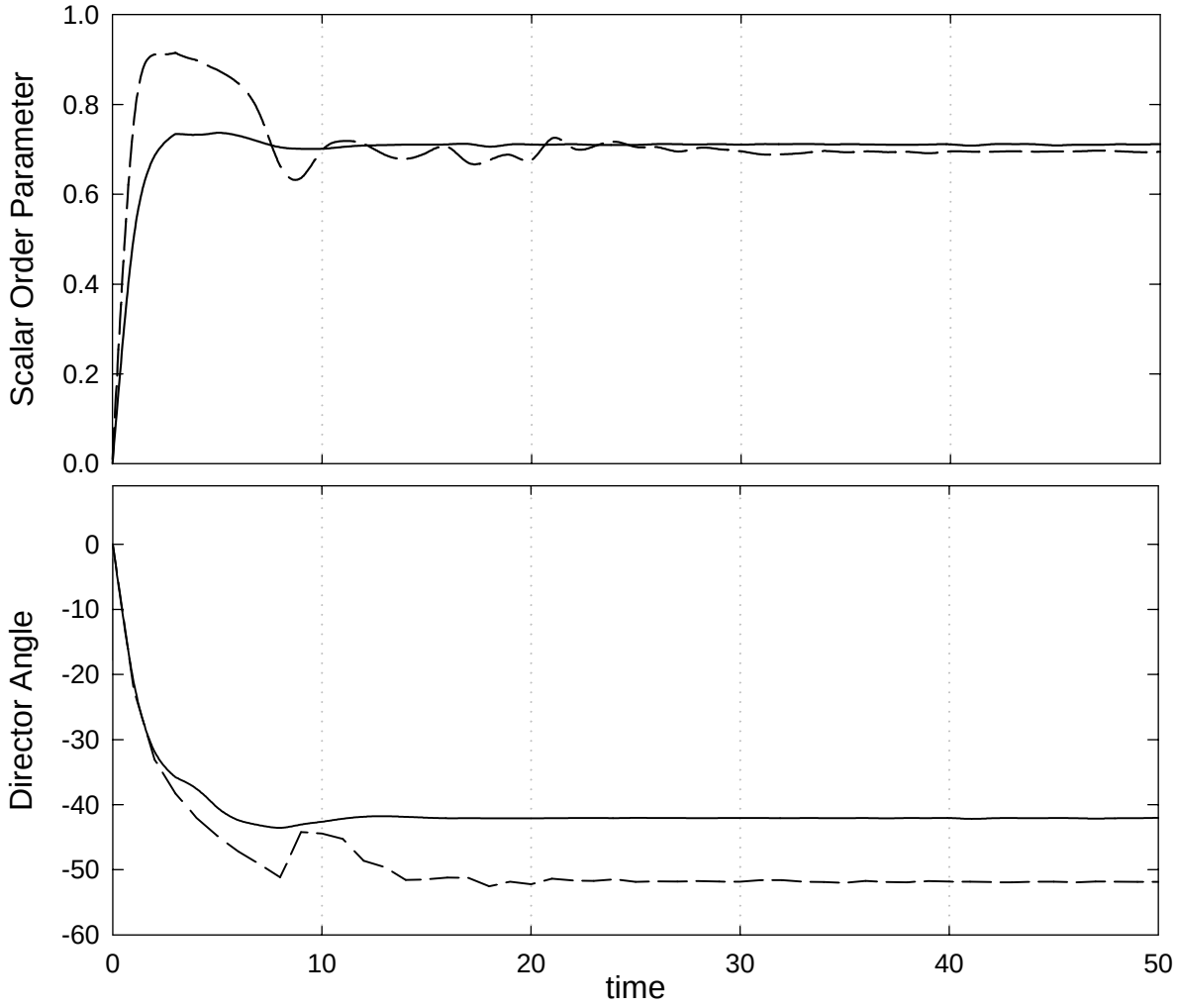

Figure 11
Grosso et al.

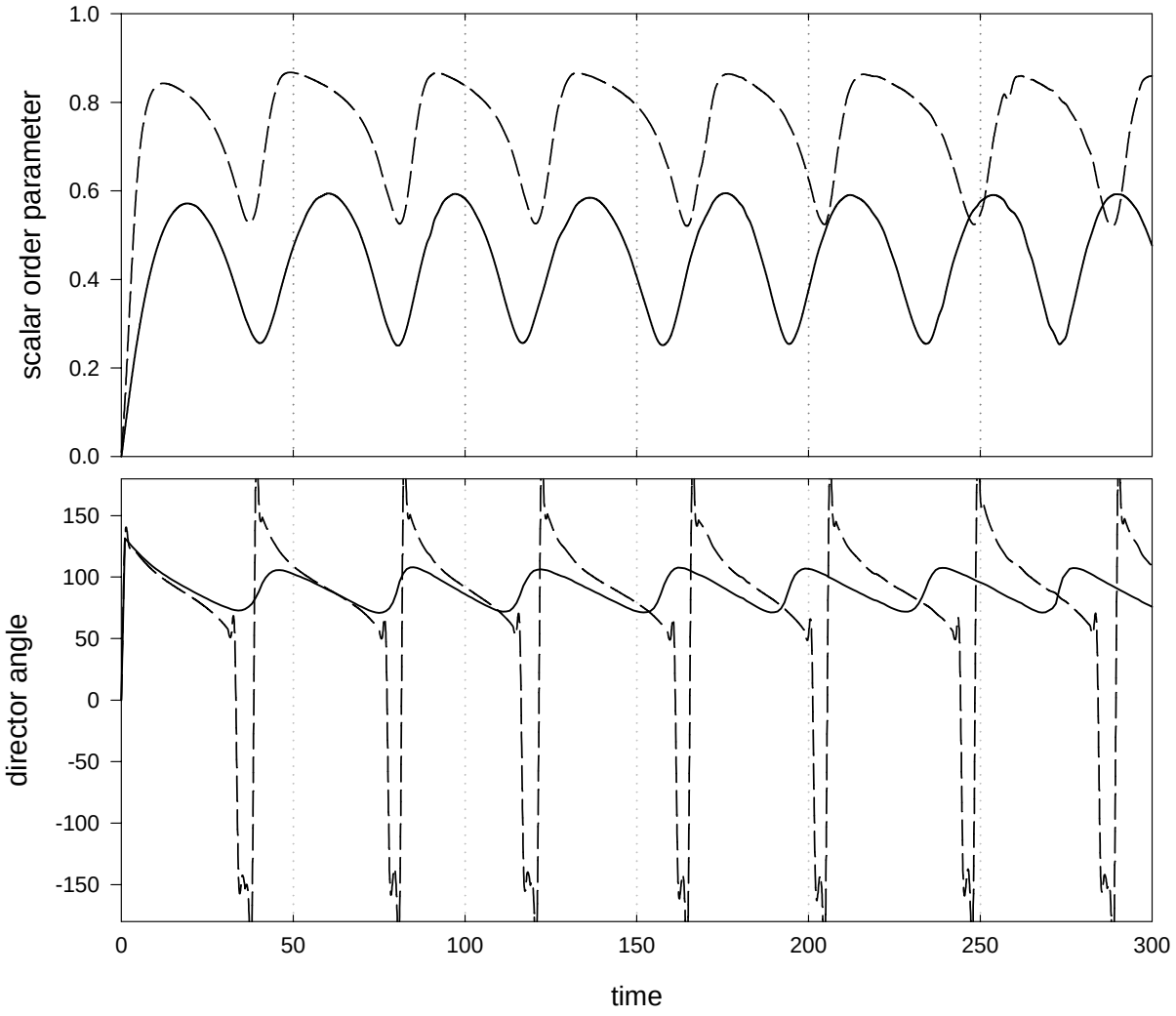

Figure 12
Grosso et al.

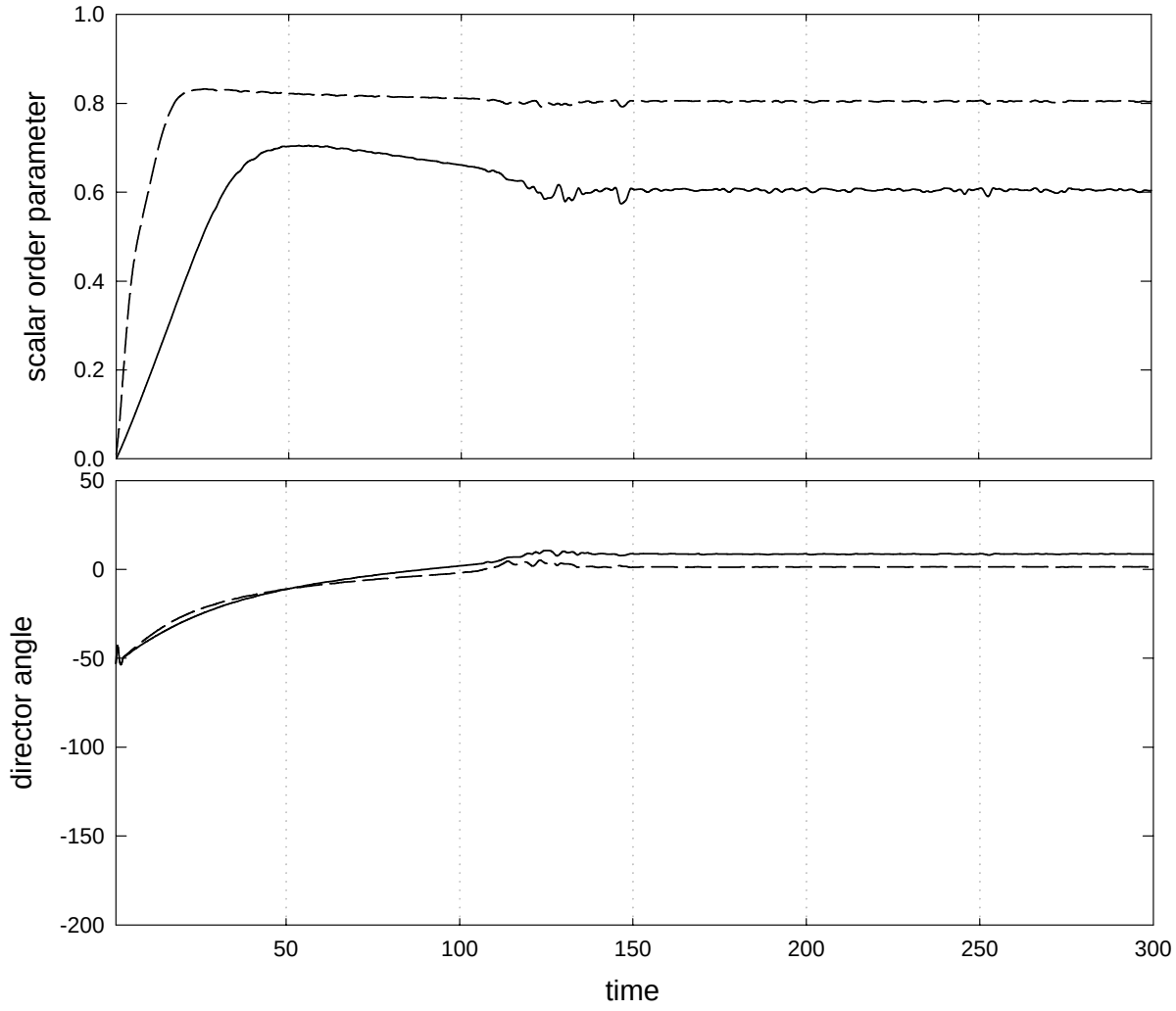

Figure 13
Grosso et al.

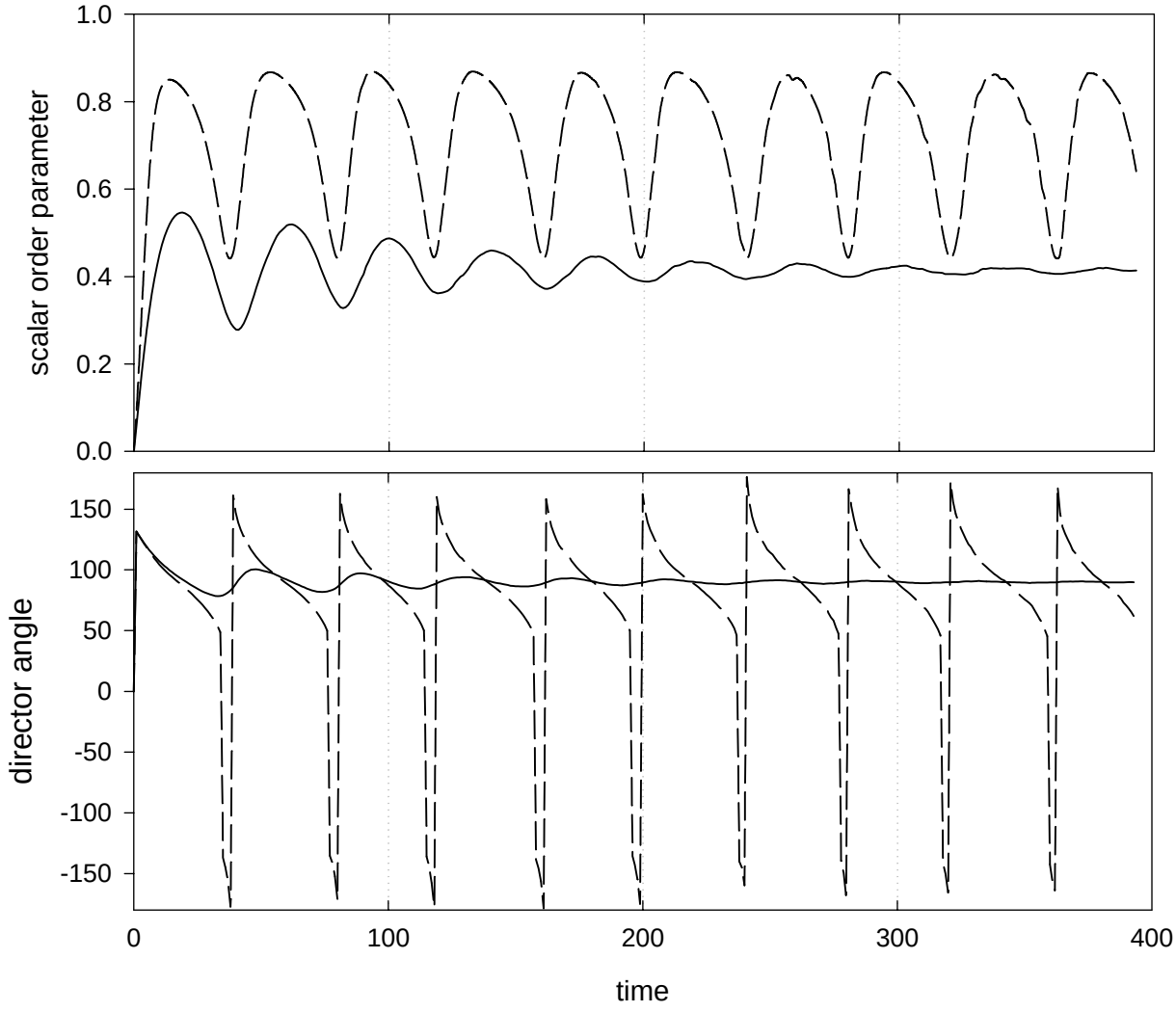

Figure 14
Grosso et al.